Tectonophysics 530-531 (2012) 299–309

Contents lists available at SciVerse ScienceDirect

Tectonophysics

journal homepage: www.elsevier.com/locate/tecto

The January 2010 Efpalio earthquake sequence in the western Corinth Gulf (Greece)

E. Sokos [a,*], J. Zahradník [b], A. Kiratzi [c], J. Janský [b], F. Gallovič [b], O. Novotny [b], J. Kostelecký [d,e], A. Serpetsidaki [a], G.-A. Tselentis [a]

[a] University of Patras, Seismological Laboratory, Greece
[b] Charles University in Prague, Faculty of Mathematics and Physics, Czech Republic
[c] Aristotle University of Thessaloniki, Department of Geophysics, Greece
[d] Czech Technical University, Faculty of Civil Engineering. Prague, Czech Republic
[e] Research Institute of Geodesy, Zdiby, Czech Republic

ARTICLE INFO

Article history:
Received 5 May 2011
Received in revised form 30 December 2011
Accepted 2 January 2012
Available online 11 January 2012

Keywords:
Corinth Gulf
Earthquake sequence
Seismicity
Focal mechanism
GPS

ABSTRACT

The January 2010 Efpalio earthquake sequence provides some key elements to enhance our view on the western Corinth Gulf tectonics. The sequence lasted almost six months, and included two Mw > 5 strong events, both exhibiting normal faulting along ~E–W trending planes. This paper attempts to construct a unified seismotectonic model of the sequence jointly interpreting earthquake locations, moment-tensors and slip inversions in terms of the possible activated fault planes. Previous studies have connected the prevailing microseismic activity to a major low-angle, north-dipping structure under the Corinth Gulf and the Efpalio sequence favors such a general trend. Moreover, it clearly shows the significance of the shallow activity, so far less recognized, and possibly connected to the relatively steep faults outcropping on the northern coast. The first 18 January 2010 Mw > 5 event had almost no on-fault aftershocks and most likely it occurred on a 55° south-dipping nodal plane. The early off-fault aftershocks formed two clusters roughly E–W trending, both of which are connected with normal faulting. Cross-sections revealed that the northernmost cluster is connected with a north-dipping structure, where the second 22 January 2010 Mw > 5 event occurred. In addition, the very shallow parts of the faults (<4 km) were mainly aseismic, probably due to their creeping behavior. Interestingly, both clusters, at their western and eastern ends, are bounded by NE-SW trending strike-slip faults, a pattern previously observed in normal-faulting structures in Greece. This observation further invokes the role of transfer faults in the western termination of Corinth Gulf, which provide the link with regional structures, such as the Trichonis and Rion-Patras fault systems. Most of all the 2010 Efpalio sequence enhanced the complex mechanical interactions within the Corinth Gulf fault network, with many earthquake generating cluster centers, an observation which has strong implications for the seismic hazard of this densely populated region.

1. Introduction

The Corinth Gulf (CG), an asymmetric graben (Fig. 1a), is often referred to as a natural laboratory for the study of continental rift tectonics (e.g. Armijo et al., 1996; Bernard et al., 2006; Doutsos et al., 1988; Hatzfeld et al., 2000; McKenzie, 1972 among many others). In fact, it is the fastest-spreading intra-continental rift on Earth, with the geodetically measured extension varying from ~5 mm/yr at the eastern part, to ~15 mm/yr at the western part (Avallone et al., 2004; Briole et al., 2000). The western CG is also characterized by a high level of microseismicity (Bourouis and Cornet, 2009). The CG is bounded by large faults along its southern coast, trending WNW-ESE to W-E and dipping steeply to the north (Doutsos and Piper, 1990; Doutsos and Poulimenos, 1992; Doutsos et al., 1988; Roberts and Koukouvelas, 1996). The northern side of the CG is bounded by a number of south dipping faults, which towards west are considered to dominate its structural evolution (Bell et al., 2008; Stefatos et al., 2002). Besides the change in rift polarity, the western part of CG is important for its tectonic link with the Rion-Patras Fault System (RPFS) to the south (Flotté et al., 2005) and the Trichonis Lake Fault System (TLFS) to the north (Fig. 1a). The link of CG to TLFS is not clearly expressed on the surface, but it has been inferred by seismological (e.g. Kiratzi et al., 2008; Melis et al., 1989) and geological studies (Vassilakis et al., 2011). On the contrary, the RPFS is clearly expressed as a NE-SW trending fault system with a mixture of dextral and dip slip kinematics, acting as a transfer system between CG and other structures parallel to CG to the south (Doutsos and Poulimenos, 1992; Flotté et al., 2005). Active faults in the study area have been carefully mapped both onshore and offshore. The most prominent one on the southern coast of CG is the Psathopyrgos fault, trending EW and dipping at about ~60° to the

* Corresponding author.
E-mail addresses: esokos@upatras.gr (E. Sokos), jz@karel.troja.mff.cuni.cz (J. Zahradník), kiratzi@geo.auth.gr (A. Kiratzi), kost@fsv.cvut.cz (J. Kostelecký).

0040-1951/$ – see front matter © 2012 Elsevier B.V. All rights reserved.
doi:10.1016/j.tecto.2012.01.005

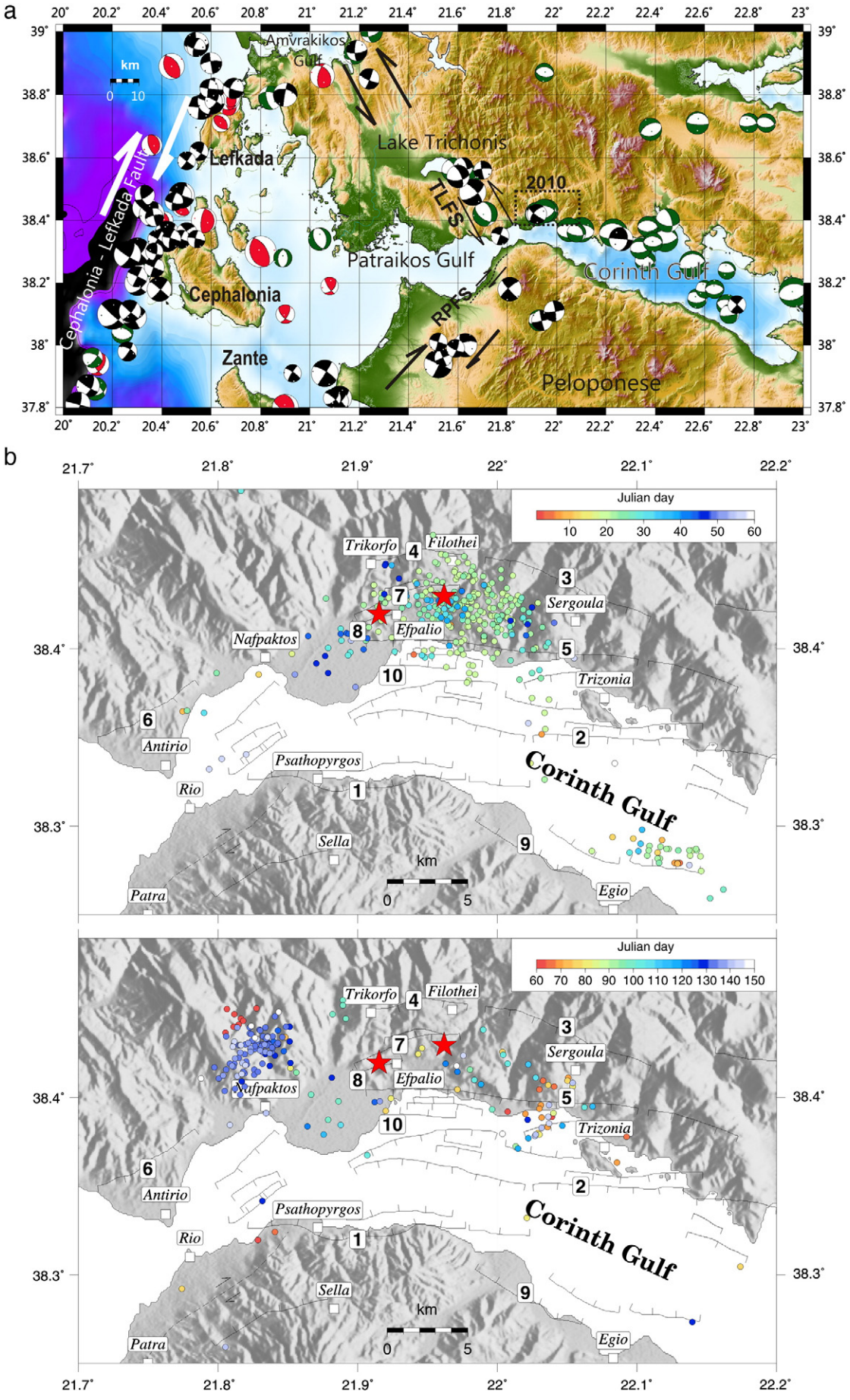
a
Amvrakikos Gulf
Lake Trichonis
Lefkada
Lefkada Fault
Cephalonia - Lefkada Fault
TLFS
2010
Patraikos Gulf
Corinth Gulf
Cephalonia
RPFS
Zante
Peloponese
km
0 10
b
Julian day
10 20 30 40 50 60
Trikorfo
Filothei
Sergoula
Efpalio
Nafpaktos
Trizonia
Antirio
Psathopyrgos
Rio
Sella
Patra
Egio
Corinth Gulf
km
0 5
Julian day
60 70 80 90 100 110 120 130 140 150

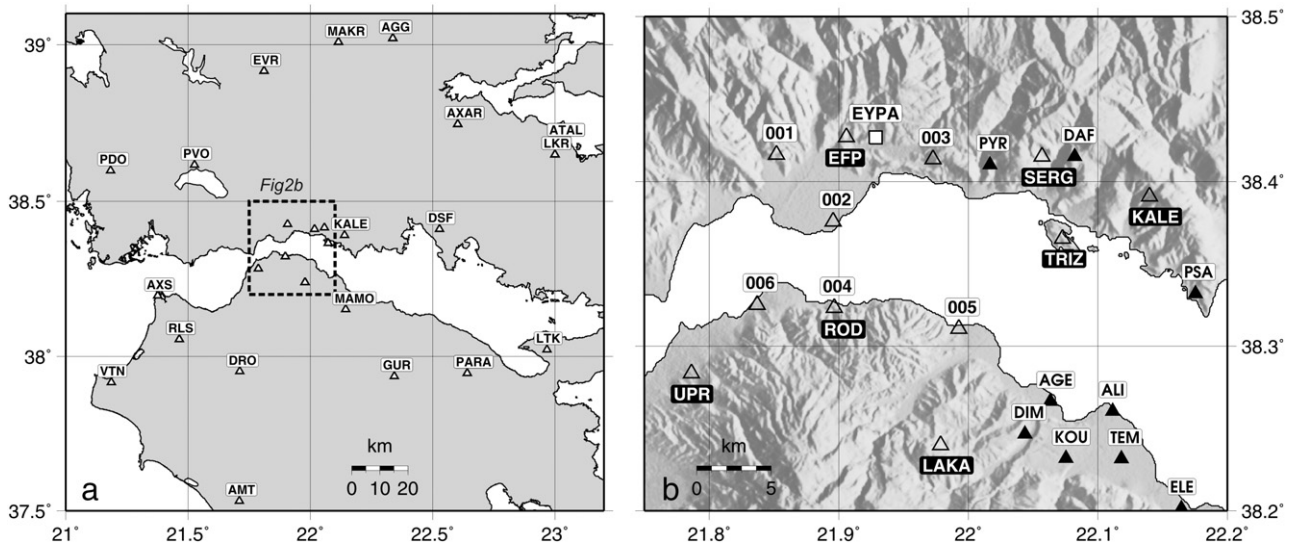

Fig. 2. a) Local and regional seismic stations, (triangles), part of the Hellenic Unified Seismic Network (HUSN), various subsets were used to locate the events in this paper and calculate their focal mechanisms. b) enhanced view of station geometry in the rectangular region shown in panel (a): HUSN stations (open triangles with letters), temporary stations of the University of Patras (open triangles with numbers), the Corinth Rift Laboratory stations (filled triangles), and the GPS station EYPA operated by CRL.

north. Towards east and closer to the city of Egio, the Selianitika fault links the Psathopyrgos fault with CG faults while towards south the Psathopyrgos fault links to Rion-Patras faults (Fig. 1b). On the northern coast, the Marathias fault dipping at about 55` to the south is the most prominent active structure, with a total length of 12 km (Gallousi and Koukouvelas, 2007; Valkaniotis, 2009). Besides normal faults with a general E-W strike there is also seismological evidence for active transfer faults connecting the major en-echelon faults (Pacchiani and Lyon-Caen, 2010; Zahradnik et al., 2004).

Even though the Corinth Gulf has been studied extensively, its westernmost part close to the Rio-Antirio strait, and especially its northern coast, it has not received enough attention. Open questions in this region, as well as for the entire Corinth Gulf, include, for example, the connection of outcropping faults to seismogenic sources at depth, the change in basin polarity (Bell et al., 2008; Stefatos et al., 2002) towards the west, the existence of a low dipping surface that controls the evolution of the gulf (Sorel, 2000), the role of off-shore faults and the activity of Psathopyrgos fault; quite important issues for the seismic hazard of this densely populated area. Regarding fault geometry two models have been proposed; either steeply-dipping faults which are joined at depth with a low-angle seismically active detachment (Rigo et al., 1996), or faults with a progressive down dip curvature, merging into low-angle detachments (Doutsos and Poulimenos, 1992; Sorel, 2000).

The aim of the present study is to address, to the degree that the available data allow, the open questions of the Corinth Gulf tectonics. To achieve this, we study in detail the spatiotemporal evolution and source characteristics of the January 2010 sequence in the northern bank of the Corinth Gulf. The two strongest events on January 18 and 22 had reported magnitudes Mw > 5 (5.5 and 5.4, respectively according to USGS/NEIC). In the following paragraphs we will refer to the event magnitudes as Mw = 5.3 and 5.2, respectively adopting the magnitude determination from our moment tensor analysis. The two events were followed by an aftershock sequence which lasted for almost six months and spread as much as ~10 km both westward and eastward (Fig. 1b). Thus, in the following we jointly interpret the event locations, moment-tensors calculations and slip inversions, partially constrained by a permanent GPS station measurement. The model will be discussed in terms of the likely activated fault structures.

2. January 18 (Ev1) and January 22 (Ev2) events

2.1. Relocation of the hypocenters for the two strongest events

On January 18, 2010 (GMT 15:56) an earthquake of Mw5.3 occurred near the town of Efpalio on the northern coast of the western Corinth Gulf. Almost immediately the seismic activity expanded ~5 km towards north-east where four days later another Mw5.2 event occurred (January 22; GMT 00:46). Both events were well recorded by the broad band stations of the Hellenic Unified Seismic Network (Fig. 2a), while on 19th January a temporary network of six short period stations was deployed in the epicentral region (Fig. 2b), whose readings greatly improved location accuracy.

The spatiotemporal evolution of the entire Efpalio sequence, as derived from locations based on manual phase picking, clearly indicates that many faults were activated, producing a complicated clustering pattern, as previously shown (e.g. Fig. 1b). In the following, we will focus on the central cluster of the sequence, approximately bounded by meridians 21.9° to 22°, and its first thirty days.

We start with a two-step relocation of the two strongest events. During the first step regional stations (up to ~70 km distance) were used to locate the epicenter, while, in the second step, the epicenter was held fixed, and the depth was grid searched to minimize the

Fig. 1. a) Regional tectonics of the Corinth and Patraikos Gulfs and available previous earthquake focal mechanisms (Kiratzi and Louvari, 2003). In the color version of the figure normal faulting is depicted by green beach-balls, thrust/reverse faulting by red beach-balls and strike-slip faulting by black beach-balls. TLFS = Trichonis Lake Fault System; RPFS = Rion-Patras Fault System. The pairs of opposing arrows denote the polarity of the strike-slip motions. The region of the 2010 Efpalio sequence is depicted within the rectangle. b) The Efpalio earthquake sequence, from January to May 2010, color scale refers to the activation time. Two time periods are shown, January to February 2010 (top panel) and March to May 2010 (bottom panel). The two largest events are shown by asterisks. Major faults shown are: 1 = Psathopyrgos, 2 = Trizonia, 3 = Trikorfo, 4 = Filothei, 5 = Marathia, 6 = Antirio, 7 = Drosato, 8 = Efpalio, 9 = Selianitika, and 10 = off shore fault related to Efpalio sequence and other on- and off-shore faults. (Fault traces as in Doutsos and Poulimenos, 1992; Flotté et al., 2005; Papanikolaou et al., 1997; Valkaniotis, 2009).

Table 1
Crustal models used in present study. Latorre model refers to crustal model proposed for the Efpalio area by Latorre et al., 2004 while Rigo model has been proposed by Rigo et al., 1996 and has been used extensively in Corinth gulf. Vp/Vs ratio value used was 1.78.

Depth (km)	Vp (km/s)
Latorre model	
0.00	4.27
2.90	5.06
3.80	5.15
4.50	5.21
5.00	5.35
6.00	5.53
6.50	5.65
7.00	5.83
7.70	6.08
8.30	6.35
9.10	6.40
16.00	6.60
33.00	8.37
Rigo model	
0.00	4.80
4.00	5.20
7.20	5.80
8.20	6.10
10.40	6.30
15.00	6.50
30.00	7.00

residuals at near stations only. The velocity model of Rigo et al. (1996) was used (Table 1). The hypocenters determined in this way are listed in Table 2 and plotted in Fig. 3a,b (stars denoted as A and A', for Ev1 and Ev2, respectively); these will serve as a reference solution. An alternative solution with the omission of a few stations and azimuthal weights is denoted as B and B', respectively. Furthermore, for Ev1, relocation was done also using a foreshock, which occurred 25 seconds before. Due to its small magnitude (ML2.5), unclipped P- and S-waves were available at near stations, whose readings constrained the foreshock depth at 6 km. Using the foreshock residuals at near stations as station corrections, we calculated the Ev1 depth at 5.9 km, close to the above two-step result (see also Fig. 3b, hypocenter D). These results are consistent with Lyon-Caen et al. (2010). The two-step approach was selected because when we made a standard one-step inversion of local and regional stations (the latter being important for a reliable epicenter position due to their good azimuthal coverage) the hypocenter was shifted to larger depths (8 to 11 km). A number of recent models for the region have a stronger velocity gradient at a depth of about 6 to 8 km (Gautier et al., 2006; Latorre et al., 2004). If, for example, the gradient model from Latorre et al., 2004 (panel *d* of their Fig. 16) is used in the Hypoinverse code (Klein, 2002), the hypocenter depths of Ev1 and Ev2 automatically move towards those listed in Table 2, (see also Fig. 3 — epicenters C and C'). Note that the depth bias from ~6 to ~9 km is also confirmed by a simple comparison with the depths derived from the moment tensor inversion of strongest aftershocks (see Section 3).

Comparing solutions A to D for Ev1 and A' to C' for Ev2 (Fig. 3a, b), we obtain a rough estimate of the possible location bounds. In fact, extensive additional trials were carried, for example, re-picking the first arrivals by different operators, using a 3D grid search, locating simultaneously with the velocity determination, jackknifing the data, applying various distance and azimuthal weights among other tests. Typically, the epicenters from all these methods remained within the bounds identified by the above sample solutions. The bounds for the inferred epicenters for Ev1 event are broader than the expected standard error estimates of any separate location method. However, these bounds are smaller for Ev2 since for this event the temporary stations were available. The effect of local stations on depth resolution is evident also in the relocation procedure described in the following paragraphs.

2.2. Centroid moment tensor (CMT) solutions

The MT inversion was performed using the ISOLA software (Sokos and Zahradnik, 2008). ISOLA calculates the moment tensor by least-squares matching complete observed waveforms with synthetics, calculated in a 1D crustal model. It is a low-frequency time-domain method working under assumption of a known moment-rate function (the delta function). Multiple sources in space and time can be considered, but here we retrieve only single-source moment tensors. Further, we assume only deviatoric sources, composed from a DC (double-couple) and CLVD (compensated linear vector dipole) part; e.g. Zahradnik et al., 2008c. The centroid position was calculated by a 3D spatial grid search. Full waveforms from eight regional stations were used in the distance range from 11 to 100 km (see Table 3 for station information). Waveforms were band-pass filtered between 0.05 and 0.10 Hz. In general, the non-double-couple percentage was quite small (<10%); therefore, reported hereafter is the double-couple focal mechanism only (see Table 4). The focal mechanism was very stable within a few kilometers of the optimum source position, both in the horizontal and vertical direction. Before the final spatial centroid search, the focal mechanisms were fixed. The global variance reduction over all three-component waveforms was typically 0.8. The centroid position and the corresponding focal mechanism, both for Ev1 and Ev2, are summarized in Table 2 and plotted in Fig. 3 as reference solutions c1 and c1', respectively. To estimate the uncertainty levels of the CMT inversion, various tests were performed which in general included: different crustal models, repeated omission of a station, variation of the frequency range, variable station weighting. Two samples of the alternative centroid positions for each event, most often encountered in these tests, are shown in Fig. 3, marked as c2, c3 and c2', c3', respectively, together with a rough estimate of their position bounds. Note that the two events have slightly different CMT's; both mechanisms indicate rupture of approximately EW trending normal faults, but Ev1 centroid is shallower than Ev2 (centroid depths are 4.5 and 6 km, respectively).

2.3. Constraining centroid depth from GPS measurements

Data of the permanent GPS station EYPA, operated by the Corinth Rift Laboratory (http://crlab.eu/) (Fig. 3a) were used in order to provide an additional constraint on the centroid depth. The GPS data were processed by the Precise Point Positioning method (software available at the Geodetic Survey Division of Geomatics, Canada http://csrsjava.geod.nrcan.gc.ca/). This method makes use of a single station

Table 2
Hypocenters and centroids calculated for the two strongest events. These values were adopted as reference solutions. (Alternative solutions are shown in Fig. 3).

Date and origin time	(H) hypocenter		H-depth (km)	(C) centroid		C-depth (km)	Seismic moment (Nm)
	Lat. (°N)	Lon. (°E)		Lat. (°N)	Lon. (°E)		
Jan 18 2010 15:56 GMT	38.419	21.915	6.6	38.422	21.941	4.5	0.97e17
Jan 22 2010 00:46 GMT	38.429	21.962	8.0	38.430	21.964	6.0	0.70e17

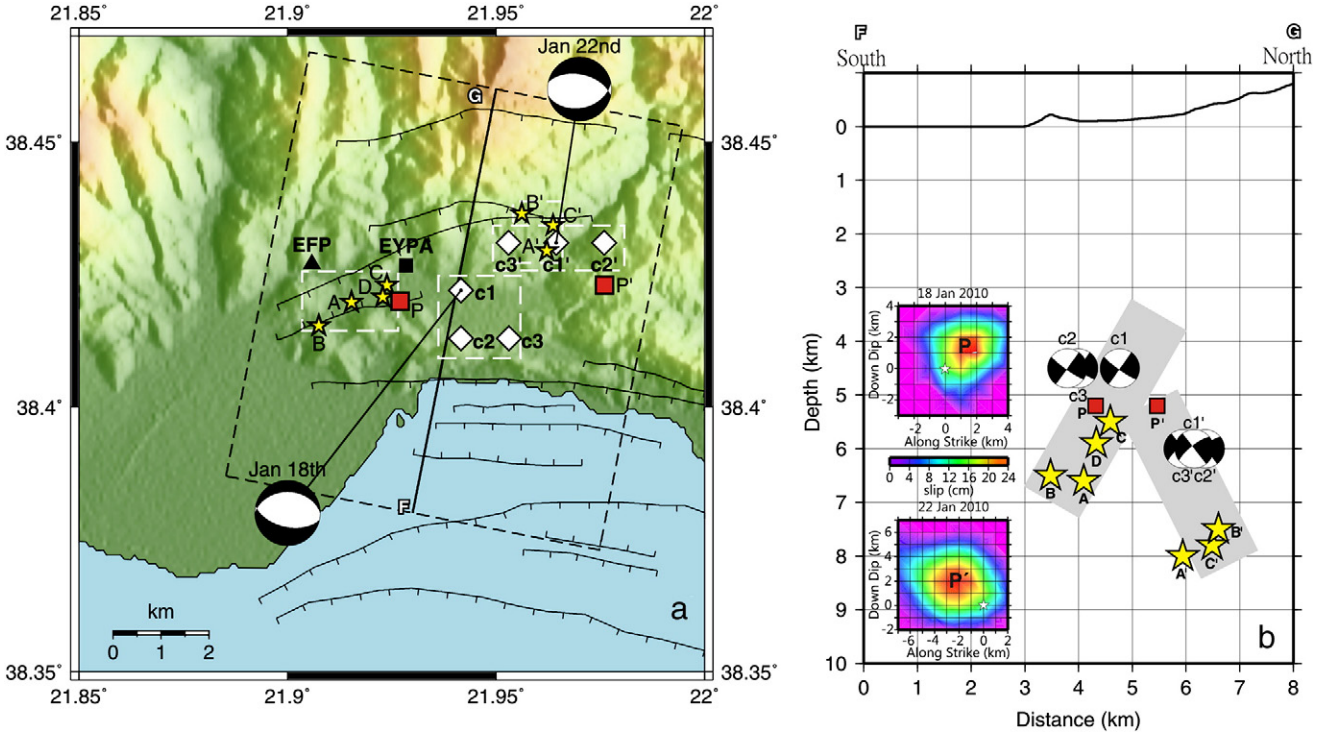

Fig. 3. Map view of epicenters and centroids for the 18 January and 22 January 2010 events; b) vertical cross-section along line FG at an angle N10°E. The gray strips schematically demonstrate the likely fault planes. In both figures the reference solutions are depicted as hypocenters A, A' and centroids c1, c1' for Jan18 event and Jan22 event, respectively (see Table 2). A few alternative positions for the hypocenters (B, C, D and B', C' for Ev1 and Ev2, respectively) and centroids (c2, c3 and c2', c3') inside the solution bounds (dashed white rectangles) are also shown and discussed in the text. Red (in the colored version) squares P and P' mark the locus of peak slip within the slip patches obtained from the inversion of regional broad band waveforms (slip models in fault coordinates are depicted in Fig. 3b inset; the white asterisks in these models mark the hypocenter positions A and A'). Slip is represented on the fault plane using a local coordinate system, along strike and along dip, with the hypocenter located at 0,0.

and satellites with only 5 cm position accuracy. The 30-s sampled data were represented by 1-day mean values. Further, the 1-day values were processed by the so-called anharmonic analysis (Vaníček, 1971), i.e., main hidden periods were detected and removed to obtain the constant values, separately for the 30 days before and after the Jan 18 event. Finally, the difference between the two values (before and after the earthquake) is what we call the GPS-measured positional change: $NS = -0.13 \pm 0.02$ cm, $EW = 1.22 \pm 0.07$ cm, $Z = -4.10 \pm 0.10$ cm. These values are in agreement with those reported by Lyon-Caen et al. (2010), i.e. 0 cm, +1 cm and −3 cm for the NS, EW and Z component, respectively. They indicate the surface motion related to the studied earthquake (−s). Similar numerical values were obtained if processing two 30-day groups while excluding, for example, 7 days, starting one day before Ev1 and terminating one day after Ev2. In other words, at this level of the data processing, it is not possible to assign the above numbers solely to the first event. Nevertheless, even at the present stage of knowledge it is interesting to note that the whole amount of the indicated change might be explained, for example, by the slip at a depth of 4.5 km, equivalent to a single event Mw 5.3 at the c1 position (Fig. 3). Indeed, if we calculate theoretical values of the static displacement in COULOMB 3.1 code (Toda et al., 2005) we obtain a fairly good agreement with the GPS observation: -0.31 cm, +0.78 cm, and −3.12 cm, for the NS, EW and Z component, respectively. Particularly well constrained is the east–west centroid position; e.g., shifting the source 2 km to the west relative to c1 would already produce a wrong sign of the EW component. Thus the estimated position of the main slip patch of Ev1 is realistic (i.e. it is not in contradiction to the GPS).

2.4. Centroid position of Ev1 and Ev2 validated by the slip inversion

In order to further validate the centroids for the Ev1 and Ev2 events we calculated the slip models of the two events, hoping that the centroids will coincide with the peak slip patches. Slip models were determined using the method of Dreger and Kaverina (2000) and Kaverina et al. (2002) as applied in other Aegean earthquakes (e.g. Benetatos et al., 2006, 2007; Kiratzi, 2011), in which regional distance ground motions recorded on broadband instruments are inverted for slip through a least squares scheme. The applied method requires simplified assumptions including constant rupture velocity and dislocation rise time and poses slip positivity, seismic moment minimization and smoothing constraints during the inversion procedure. The slip models were obtained on planes passing through the hypocenter positions (Table 2), using the strike, dip and rake angles of the MT solutions (Table 4). Both nodal planes were tested in the inversions, but finally we adopted the planes providing better waveform misfit, i.e. the south dipping plane for the first event (Ev1) and the north dipping plane for the second event (Ev2). The slip models for these nodal planes are shown here (Fig. 3b inset). As expected

Table 3
Stations used in the moment tensor inversion, with the corresponding epicentral distances and azimuths. The operating institutes are the Corinth Rift Laboratory (CRL-IPGP) in cooperation with the University of Athens (UOA), the University of Patras -Seismological Laboratory (UPSL), the Charles University in Prague (CUP), the Geodynamic Institute, National Observatory of Athens (GI-NOA). All stations are part of the Hellenic Unified Seismological Network (HUSNET).

Station	Distance (km)	Azimuth (°)	Operating Institute
TRIZ	13	119	CRL-IPGP/UOA
MAMO	35	149	UPSL/CUP
DSF	51	91	UPSL
DRO	56	201	UPSL
EVR	56	348	GI-NOA
GUR	64	147	UPSL
PDO	69	287	UPSL/CUP
LTK	100	116	UPSL/CUP

Table 4
Focal mechanism solutions for the Efpalio 2010 sequence. For Ev1 and Ev2 the spatial positions obtained by CMT determination are listed. For the rest of the events the kinematic locations of the epicenter are listed, and moment tensors were determined by grid-searching the depth. Paz = P-axis azimuth, Ppl = P-axis plunge, Taz = T-axis azimuth, Tpl = T-axis plunge, VR = variance reduction, No = number of stations used in moment tensor inversion. Bold and italics are used in order to distinguish the largest events of the sequence. Their properties are discussed extensively in the text.

	YYYY	MM	DD	HH:MM:SEC	LAT (°N)	LON (°E)	DEPTH (km)	Mw	Nodal plane 1			Nodal plane 2			P axis		T axis		VR	No
									STRIKE	DIP	RAKE	STRIKE	DIP	RAKE	Paz	Ppl	Taz	Tpl		
Ev1	***2010***	***01***	***18***	***15:56:09.80***	***38.422***	***21.941***	***4.5***	***5.3***	***102***	***55***	***−83***	***270***	***36***	***−100***	***39***	***79***	***187***	***10***	***0.80***	***8***
1	2010	01	18	16:16:13.87	38.410	22.004	12.4	3.5	290	77	−57	39	35	−157	235	48	355	25	0.58	9
2	2010	01	18	17:10:13.14	38.435	21.977	10.5	3.7	293	72	−61	52	34	−146	239	54	1	22	0.72	8
3	2010	01	18	17:20:11.15	38.416	22.002	7.8	3.5	252	89	−172	162	82	−1	117	6	27	5	0.55	8
4	2010	01	18	17:27:06.31	38.437	21.972	9.4	3.5	42	51	170	138	82	39	264	20	8	33	0.41	9
5	2010	01	18	17:35:35.84	38.430	21.983	9.5	3.2	289	77	−39	29	52	−164	242	36	344	16	0.61	10
6	2010	01	18	18:11:12.59	38.429	21.976	8.5	3.4	296	70	−49	47	45	−151	250	48	357	15	0.64	10
7	2010	01	18	20:36:56.15	38.432	21.985	10.0	3.3	247	63	−115	113	36	−50	116	63	355	15	0.21	9
8	2010	01	18	23:17:54.21	38.417	21.963	9.3	3.4	93	55	−90	273	35	−90	3	80	183	10	0.41	9
9	2010	01	19	03:45:55.14	38.429	21.982	9.6	3.4	269	34	−170	171	84	−56	112	41	234	31	0.27	7
10	2010	01	19	06:52:33.79	38.420	21.965	7.8	3.0	80	35	−93	264	55	−88	183	80	352	10	0.32	7
11	2010	01	20	07:32:36.71	38.413	21.968	8.3	3.3	56	48	−84	227	42	−97	18	85	142	3	0.18	5
12	2010	01	20	07:54:32.65	38.439	21.953	6.8	3.1	275	56	−65	55	41	−122	237	68	347	8	0.45	11
13	2010	01	21	13:42:55.15	38.415	21.984	7.8	3.5	194	90	136	284	46	0	248	29	140	29	0.69	11
Ev2	***2010***	***01***	***22***	***00:46:56.70***	***38.431***	***21.964***	***6.0***	***5.2***	***282***	***52***	***−75***	***78***	***40***	***−109***	***244***	***77***	***1***	***6***	***0.80***	***8***
14	2010	01	22	00:57:01.16	38.414	21.964	8.0	3.3	27	14	−171	288	88	−76	212	45	5	41	0.33	10
15	2010	01	22	01:27:14.76	38.428	21.955	8.5	3.5	247	31	−110	90	61	−78	27	72	172	15	0.37	11
16	2010	01	22	03:43:56.44	38.448	21.951	8.8	3.2	260	58	−83	67	33	−101	191	76	345	13	0.41	11
17	2010	01	22	04:37:35.28	38.444	21.973	7.5	3.8	268	77	−101	129	17	−50	164	57	7	31	0.20	9
18	2010	01	22	06:12:10.94	38.440	22.009	9.1	3.0	57	86	172	148	82	4	103	3	12	9	0.34	5
19	2010	01	22	10:53:32.06	38.425	21.912	9.2	4.0	37	89	141	128	51	1	90	26	345	27	0.37	10
20	2010	01	22	10:59:15.44	38.424	21.915	9.3	4.4	127	78	−28	223	63	−167	82	28	177	10	0.89	5
21	2010	01	22	12:42:34.91	38.431	21.986	7.7	3.3	311	83	−79	73	13	−147	233	51	31	37	0.34	10
22	2010	01	22	18:14:17.74	38.445	21.979	7.3	3.9	282	65	−67	57	33	−130	228	63	355	17	0.47	9
23	2010	01	22	01:20:15.06	38.438	21.972	8.5	3.5	328	70	−77	114	24	−122	259	63	48	24	0.24	11
24	2010	01	22	04:43:37.94	38.449	21.977	7.2	3.2	287	56	−38	41	59	−139	255	49	163	2	0.28	11
25	2010	01	22	07:30:08.34	38.445	21.957	8.7	3.3	272	55	−84	82	35	−98	203	79	358	10	0.37	10
26	2010	01	22	08:19:49.46	38.447	21.975	7.5	3.6	278	57	−72	67	37	−116	232	72	355	10	0.77	9
27	2010	01	29	07:44:03.76	38.398	22.010	6.2	2.5	331	60	−50	116	83	−16	251	8	344	17	0.43	4
28	2010	02	6	11:30:52.73	38.453	21.936	6.9	3.4	29	72	153	270	36	−100	188	42	40	43	0.56	7
29	2010	02	8	11:29:24.56	38.420	21.959	6.7	3.3	284	60	−62	57	40	−129	242	63	354	11	0.63	5
30	2010	02	16	08:48:57.58	38.446	21.924	7.2	2.9	208	74	−173	116	83	−16	71	16	163	6	0.25	3

for M~5, the slip models for both events (Fig. 3b inset) show, for the better fitting nodal planes, that the peak slip was confined in a small patch, best represented by its central point (squares denoted as P and P' in Fig. 3b). The agreement with the centroid positions, included in the cross section of Fig. 3b, is fairly good. Such a validation is important because the two methods are complementary. Indeed, the slip inversion automatically provides the H-C consistent solution (Zahradnik et al., 2008a). On the contrary, the CMT method grid-searches the centroid in 3D, fully independently of the hypocenter position, origin time and rupture velocity, which is an advantage when the hypocenter is not exactly known and the rupture velocity is possibly non-constant (Gallovic and Zahradnik, 2011; Zahradnik and Gallovic, 2010).

3. Relocation of the aftershocks and determination of their moment tensors

The records of the regional stations were used to locate the strongest, with M > ~3.5, aftershocks of the sequence, with the station distribution as in Fig. 2a, for the period 18 January to 17 February 2010. These were 125 events in total, and we enriched the dataset with 96 smaller magnitude (M~2.5) events, using also the records of the temporary stations at epicentral distances up to 20 km, with the network geometry as depicted in Fig. 2b, for the 19th and 20th of January. Manual picks were used in all cases, while special attention was paid to include good quality S-picks from the stations at smaller distances, in order to obtain good depth resolution. The strongest events were used in order to capture the sequence evolution, while the smaller events were used to enhance the location accuracy and to check the aftershock distribution related to the first strong event (Ev1).

Initial location was performed using Hypoinverse code (Klein, 2002) using the gradient crustal model of Latorre et al. (2004) (see Table 1). Furthermore, the HypoDD relocation method (Waldhauser, 2001) was applied, using the same velocity model, to further refine the relative location of the sequence. The catalog of P and S phase arrival times was used for double difference calculations and the system of double-difference equations was solved using the singular value decomposition (SVD) method; the derived location error estimates were of the order of a few hundred meters. The HypoDD processing included also the two strongest events, Ev1 and Ev2. Their epicenters were found within 1 km relative to those of Table 2. However, the hypocenter depth of Ev1 was ~3 km deeper, than the reference solution. The reason is again the inadequacy of the crustal model leading to biased depths when location has to rely on near and distant stations simultaneously. This led us to apply a common ~3-km shift upwards to all HypoDD obtained depths for those events that did not have enough picks to be located using near stations only. This correction was applied to 30 events out of 202 in total.

To further justify the 3-km common upward shift of the aftershocks, we compared the HypoDD derived depths to: i) the depths independently obtained from moment tensor inversion for 30 aftershocks for their moment-tensors (MT) and ii) to the depths obtained when we used the temporary local stations only.

The ISOLA software was used for the centroid moment-tensor determination for selected aftershocks. The frequency range used was up to 0.2 Hz, slightly varying through the events, and the results are summarized in Table 4. The method includes a grid search of the MT (centroid) depth. For small events the centroid and hypocenter are close to each other, but the MT depth may often be more reliable than the location depth. This is due to the fact that the relatively low-frequency MT inversion is less sensitive to the subsurface

details of the adopted crustal model (Zahradnik et al., 2008b). The comparison showed that, indeed, the MT depths were systematically shallower than the HypoDD depths, on average by 3.4 km, justifying our previously mentioned 3-km upward shift. Furthermore, the location depths obtained using local stations only and the depths from MT inversion agree very well (~1 km difference) providing a further argument for upward shift of events not having enough picks for local stations (e.g. events that occurred during the 18th and 19th of January).

4. Synthesizing the seismological data

Here we combine diverse parameters of the Efpalio 2010 sequence, such as hypocenters, centroids, and focal mechanisms, including the two strongest events and their aftershocks. The intention is to build-up a possible unified seismotectonic model of the sequence in terms of the likely fault planes.

4.1. The Ev1 and Ev2 fault planes

Discriminating the fault plane out of the nodal planes is not a simple task. For example, the GPS measurement does not prefer any of the two nodal planes of Ev1 because the relatively small finite fault of M~5 behaves practically as a point source. However, we can focus on the hypocenter (H) and centroid (C) positions from the purely geometrical viewpoint of the H-C method (Zahradnik et al., 2008a). The idea is that from two planes passing through C, and having strike

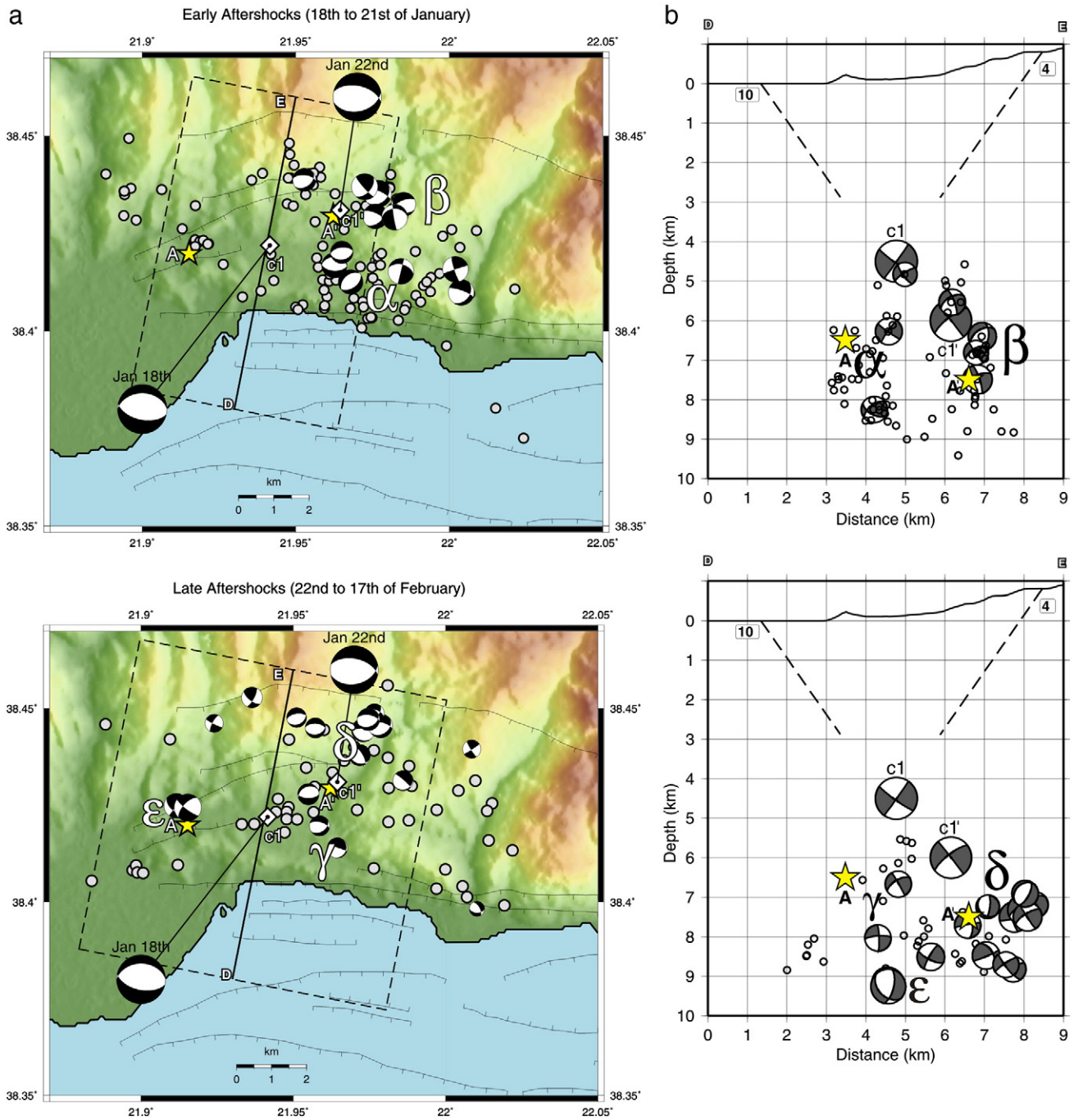

Fig. 4. Aftershocks and (selected) focal mechanisms: a) map view, and b) cross section N10°E. Top panels depict the early aftershocks, denoted α and β (between the occurrence of Ev1 and Ev2) while lower panels depict the later aftershocks, denoted γ, δ and ε (after the occurrence of Ev2 and up to February 17). Fault traces drawn on cross sections follow the numbering used in Fig. 1b.

and dip of the corresponding MT solution, the likely fault plane is the one encompassing the independently obtained H, or passing near H. Accordingly, the comparison of the alternative hypocenter and centroid positions of the 18 January 2010 (Ev1) event using an N10°E oriented vertical cross-section (e.g. Fig. 3b) favors the south-dipping fault plane (strike 102°, dip 55°), while the 22 January 2010 (Ev2) event seems to be related with the north-dipping plane (strike 282°, dip 52°). Note that for both events the centroid is at a shallower depth than hypocenter, as expected for normal faulting events (Mai et al., 2005).

4.2. Early aftershocks of Ev1 (up to the occurrence of Ev2)

The aftershocks with ML>2 are further discussed separately for the early stage, between Ev1 and Ev2, and for the later stage, after Ev2. The map-view distribution of the early aftershocks (Fig. 4a top panel) is quite irregular. Close to Ev1 centroid there are just few events. The size of such a 'gap' is in rough agreement with the assumed fault size ~4 km×4 km, based on the empirical relation between the seismic moment and the fault size (Somerville et al., 1999). Thus, Ev1 can be interpreted as a relatively simple rupture, generating almost no on-fault aftershocks (i.e. no aftershocks on the ruptured part of the fault). The early aftershocks occurred preferentially in two groups, south-east (α) and north-east (β) of Ev1. The south-east group fits with the Ev1 interpretation in terms of the south-dipping plane (Fig. 4b). These aftershocks are probably situated off the fault rupture, although geometrically are on the same plane; otherwise the rupture plane length would be too large ~6 km. This cluster (α) could mark the eastern end of the ruptured fault plane.

The north-east group (β) is clearly clustered close to place where the second event Ev2 occurred. In the map view (Fig. 4a), the cluster is situated near the likely NE termination of the horizontal projection of the Ev1 fault plane. In the cross-section (Fig. 4b), the aftershocks are located below the NE termination of the Ev1 fault. Most of the events in this cluster have a normal-faulting mechanism, featuring an almost constant strike (~280°) and dip (~67°). The dip angle is consistent with the geometry (i.e. the along-dip elongation) of the cluster (β). Hypocenter and centroid of Ev2 then followed the aftershocks within the depth range of this cluster, mapping altogether the north-dipping fault plane.

4.3. Later aftershocks (up to February 17)

Interpretation of aftershocks occurring after Ev2 is difficult. It can hardly be made in terms of the two strongest events, since both Ev1 and Ev2 might have contributed. Both in the map and cross-section view of Fig. 4 a few clusters of events appear and seem to spread out of the Ev1-Ev2 focal area, with the exception of a cluster marked with (γ) in Fig. 4a, which occurs close to Ev1 centroid location. What is well seen from the map view (Fig. 4a) is the sharp termination of seismicity to the west (close to cluster (ε)), which is also marked by a series of strike-slip mechanisms. These strike-slip mechanisms mark a boundary at the west of the sequence with a NNE strike. A similar, but less pronounced boundary, seems to exist at the eastern termination of the sequence, where a few strike-slip mechanisms appear also (Fig. 4a, b). Finally, during this later phase of the sequence the existence of a sub parallel surface at the depth of 8–9 km is marked by seismicity and focal mechanisms. This is most probably connected with the detachment zone proposed by Rigo et al. (1996), or with the brittle–ductile transition zone according to Hatzfeld et al. (2000).

4.4. Static Coulomb stress changes: Ev2 triggered by Ev1

The above mentioned cluster (β) of the early off-plane Ev1 aftershocks, and its proximity to Ev2, is a strong indication that these events were triggered by a stress perturbation due to Ev1. To analyze such a situation, the Coulomb stress was calculated using COULOMB 3.1 code (Toda et al., 2005). Shown in Fig. 5 is the map view (at the depth of 6.5 km, i.e. 2 km below the first strong event centroid, and the N10°E vertical cross section passing slightly (0.5 km) off the assumed rupture area. The stress was resolved assuming focal mechanism of Ev2, (e.g. 282°, 52°, 75°). Good correlation of the early aftershocks occurrence with the positive stress change is evident, for both clusters (α) and (β). It confirms the above mentioned assumed triggering of Ev2 by Ev1 and provides further evidence for fault interaction in this tectonically complex area. Another important result of the Coulomb analysis is that the shallow part, above Ev1, was also experiencing the positive stress change, but no aftershocks were located there. Indeed, all studied aftershocks are localized solely at the depths greater than the main slip release (i.e. they are absent at the depths shallower than 4–5 km), with possible interpretation in terms of creeping shallow segments of the faults (see for example Bernard et al., 2006).

5. Discussion and conclusion

We used high quality seismic data to relocate the Efpalio 2010 sequence, determined the focal mechanisms and centroid positions of the two strongest events and major aftershocks, and synthesized all results in a seismotectonic model. To summarize, we arrived at the following scenario of the studied part of the sequence (18 January 2010 to 17 February 2010). The first strong event (Ev1) had almost no aftershocks close to the main ruptured region. The relative position of hypocenter and centroid, as well as the spatial distribution of the early aftershocks, indicate that Ev1 ruptured a south-dipping plane.

The early aftershocks formed two separate clusters, both likely provoked by the Coulomb stress. Cluster (β) in Fig. 4, represents a north-dipping structure at which, later, the second strong event (Ev2) occurred. After the occurrence of Ev2, seismicity started to spread out of the Ev1-Ev2 focal area. The sequence termination towards north-east and south-east is marked by strike-slip mechanisms, illustrating the effect of the faults striking in the SW–NE direction, a picture also seen in other normal faulting sequences in Greece (for example the Kozani 1995 sequence, e.g. Fig. 6 from Papazachos et al., 1998).

These deep structures, based solely on seismological data, may be related to mapped surface traces of faults. For example, if we upward extrapolate the constant fault dip to the surface, the surface trace for the south dipping fault of Ev1 is very well correlated with the Trikorfo-Filothei south dipping fault (nos. 3 and 4 in Fig. 1b). Similarly the extrapolated surface termination of the assumed causative fault for Ev2 is located offshore, close to the north-dipping fault (no. 10 in Fig. 1b) mapped by Papanikolaou et al. (1997) during a sea bottom survey.

This interpretation can be compared with proposed models for western Corinth Gulf. For example, Latorre et al. (2004) and Gautier et al. (2006) located many small earthquakes by dense temporary networks, and made tomography investigations. These authors have consistently reported a general trend in seismicity of the western part of the Corinth Gulf, marked by weak earthquakes that follow a low-angle north-dipping structure. This structure is understood as a continuation of the relatively steeply dipping normal faults outcropping at the southern coast. The comparison of our results with such a major north-dipping structure is shown in Fig. 6. It is evident that the 2010 Efpalio sequence does not significantly deviate from the general trend, except one important aspect: this sequence clearly proved also a shallower activity on the northern coast, possibly related with the relatively steeply dipping surface faults. The deeper part of the Efpalio sequence correlates with an almost flat structure at the depth of ~8 km. In this sense, the sequence illuminated a possible connection of the major north-dipping active structure under the Corinth Gulf to the relatively shallow, steep faults located

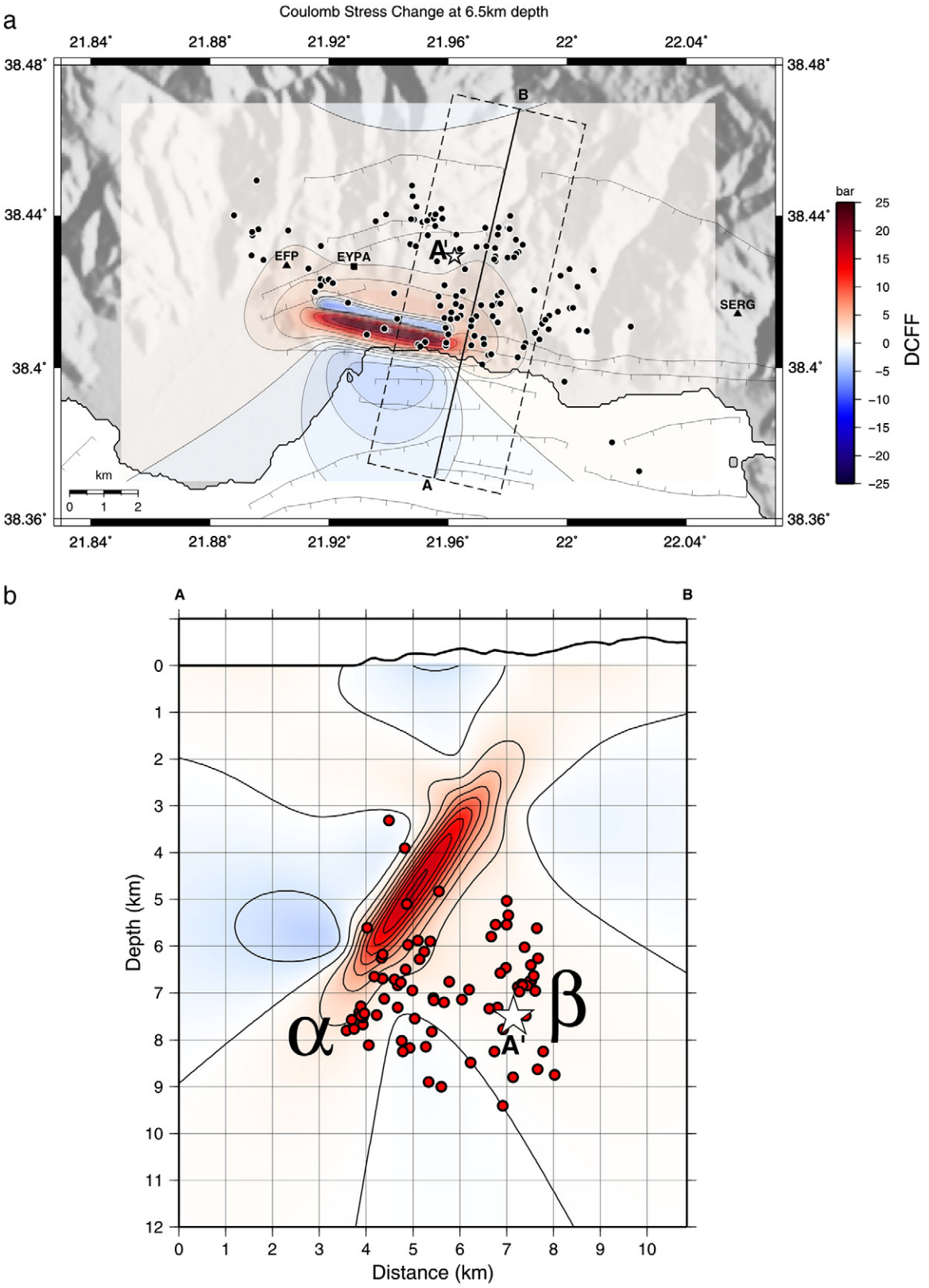

Fig. 5. The Coulomb stress change due to the first strong event, Ev1: a) map view at a depth of 6.5 km, i.e. 2 km below the centroid depth, and b) vertical cross-section passing 0.5 km from the eastern termination of the assumed south-dipping fault plane. Shown are also the early aftershocks (circles), denoted α and β as in Fig. 4 and the second strong event, Ev2 (star denoted as A'). Note their tight relation with the positive stress change.

on its northern coast and offshore. The term "relatively shallow seismically active structures" should be understood with caution. We mean the depths, between ~4 km and 7 km, but not shallower than 4 km. The absence of aftershocks at the depths smaller than 4 km is also important; it indicates no motion or a creep behavior of the very shallow part of the faults.

Finally, let us try to characterize the Efpalio sequence in the regional scale, i.e. we discuss how it relates to major regional structures

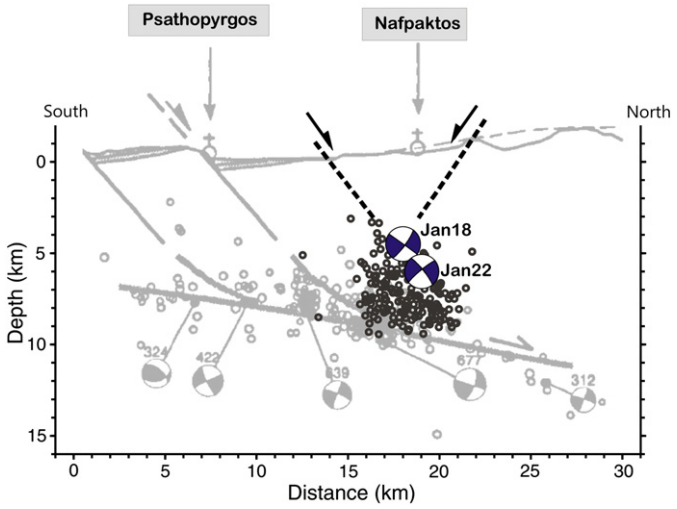

Fig. 6. N–S cross section along the western Corinth Gulf depicting previous seismicity (gray circles) and focal mechanisms (Fig. 12 from Rigo et al., 1996); the hypocenters (black circles) and focal mechanisms of the Efpalio sequence are superimposed. The comparison of the new data regarding the major north-dipping structure under the Corinth Gulf shows that the Efpalio sequence did not deviate from a general trend of seismic activity below the Gulf, but it emphasizes a link with shallower, more steeply dipping fault structures of the northern coast.

mentioned in the introduction. In this context, the most important is the above described finding that the sequence was related to almost parallel normal faults, displaced with each other by strike-slip faults (while the latter also affected the sharp spatial termination of the activity). The entire pattern seems to fit well in a regional tectonic system (Fig. 1a). Furthermore we could speculate that the relatively shallow seismicity in this part of the Corinth Gulf is connected with shallow young faults marking the continuation of the rift towards the west and the connection with either the Trichonis Lake Fault System (TLFS) or the Rion-Patras Fault System (RPFS). The above results provide further evidence for the triple junction character of the western Corinth Gulf suggested recently by Vassilakis et al. (2011).

Acknowledgments

The authors acknowledge the data exchange between the Patras University (including the joint Patras-Prague stations), the Corinth Rift Laboratory network (CRL-IPGP), and the Hellenic Unified Seismic Network (HUSN). Helene Lyon-Caen, Anne Deschamps and Pascal Bernard provided useful discussions. GPS data of the permanent station EYPA, operated under CRL by Pierre Briole were used (http://crlab.eu/). This study was partially supported by the following grants: GACR 210/11/0854 and MSM 0021620860 in the Czech Republic.

Appendix A. Supplementary data

Supplementary data to this article can be found online at doi:10.1016/j.tecto.2012.01.005.

References

Armijo, R., Meyer, B., King, G.C.P., Rigo, A., Papanastassiou, D., 1996. Quaternary evolution of the Corinth Rift and its implications for the Late Cenozoic evolution of the Aegean. Geophysical Journal International 126 (1), 11–53. doi:10.1111/j.1365-246X.1996.tb05264.x.

Avallone, A., Briole, P., Agatza-Balodimou, A.M., Billiris, H., Charade, O., Mitsakaki, C., Nercessian, A., Papazissi, K., Paradissis, D., Veis, G., 2004. Analysis of eleven years of deformation measured by GPS in the Corinth Rift Laboratory area. Comptes Rendus Geosciences 336 (4–5), 301–311. doi:10.1016/j.crte.2003.12.007.

Bell, R.E., McNeill, L.C., Bull, J.M., Henstock, T.J., 2008. Evolution of the offshore western Gulf of Corinth. Geological Society of America Bulletin 120 (1–2), 156–178. doi:10.1130/b26212.1.

Benetatos, C., Kiratzi, A., Ganas, A., Ziazia, M., Plessa, A., Drakatos, G., 2006. Strike-slip motions in the Gulf of Sigaçik (western Turkey): properties of the 17 October 2005 earthquake seismic sequence. Tectonophysics 426 (3–4), 263–279. doi:10.1016/j.tecto.2006.08.003.

Benetatos, C., Dreger, D., Kiratzi, A., 2007. Complex and segmented rupture associated with the 14 August 2003 Mw 6.2 Lefkada, Ionian Islands, earthquake. Bulletin of the Seismological Society of America 97 (1B), 35–51. doi:10.1785/0120060123.

Bernard, P., Lyon-Caen, H., Briole, P., Deschamps, A., Boudin, F., Makropoulos, K., Papadimitriou, P., Lemeille, F., Patau, G., Billiris, H., Paradissis, D., Papazissi, K., Castarède, H., Charade, O., Nercessian, A., Avallone, A., Pacchiani, F., Zahradnik, J., Sacks, S., Linde, A., 2006. Seismicity, deformation and seismic hazard in the western rift of Corinth: new insights from the Corinth Rift Laboratory (CRL). Tectonophysics 426 (1–2), 7–30. doi:10.1016/j.tecto.2006.02.012.

Bourouis, S., Cornet, F.H., 2009. Microseismic activity and fluid fault interactions: some results from the Corinth Rift Laboratory (CRL), Greece. Geophysical Journal International 178 (1), 561–580. doi:10.1111/j.1365-246X.2009.04148.x.

Briole, P., Rigo, A., Lyon-Caen, H., Ruegg, J.C., Papazissi, K., Mitsakaki, C., Balodimou, A., Veis, G., Hatzfeld, D., Deschamps, A., 2000. Active deformation of the Corinth rift, Greece: results from repeated Global Positioning System surveys between 1990 and 1995. Journal of Geophysical Research 105 (B11), 25605–25625. doi:10.1029/2000jb900148.

Doutsos, T., Piper, D.J.W., 1990. Listric faulting, sedimentation, and morphological evolution of the Quaternary eastern Corinth rift, Greece: first stages of continental rifting. Geological Society of America Bulletin 102 (6), 812–829. doi:10.1130/0016-7606(1990) 102<0812:lfsame>2.3.co;2.

Doutsos, T., Poulimenos, G., 1992. Geometry and kinematics of active faults and their seismotectonic significance in the western Corinth-Patras rift (Greece). Journal of Structural Geology 14 (6), 689–699. doi:10.1016/0191-8141(92)90126-h.

Doutsos, T., Kontopoulos, N., Poulimenos, G., 1988. The Corinth-Patras rift as the initial stage of continental fragmentation behind an active island arc (Greece). Basin Research 1 (3), 177–190. doi:10.1111/j.1365-2117.1988.tb00014.x.

Dreger, D., Kaverina, A., 2000. Seismic remote sensing for the earthquake source process and near-source strong shaking: a case study of the October 16, 1999 Hector Mine earthquake. Geophysical Research Letters 27 (13), 1941–1944. doi:10.1029/1999gl011245.

Flotté, N., Sorel, D., Müller, C., Tensi, J., 2005. Along strike changes in the structural evolution over a brittle detachment fault: example of the Pleistocene Corinth-Patras rift (Greece). Tectonophysics 403 (1–4), 77–94. doi:10.1016/j.tecto.2005.03.015.

Gallousi, C., Koukouvelas, I.K., 2007. Quantifying geomorphic evolution of earthquake-triggered landslides and their relation to active normal faults. An example from the Gulf of Corinth, Greece. Tectonophysics 440 (1–4), 85–104. doi:10.1016/j.tecto.2007.02.009.

Gallovic, F., Zahradnik, J., 2011. Toward understanding slip inversion uncertainty and artifacts: 2. Singular value analysis. Journal of Geophysical Research 116 (B2), B02309. doi:10.1029/2010jb007814.

Gautier, S., Latorre, D., Virieux, J., Deschamps, A., Skarpelos, C., Sotiriou, A., Serpetsidaki, A., Tselentis, A., 2006. A new passive tomography of the Aigion area (Gulf of Corinth, Greece) from the 2002 data set. Pure and Applied Geophysics 163 (2), 431–453. doi:10.1007/s00024-005-0033-7.

Hatzfeld, D., Karakostas, V., Ziazia, M., Kassaras, I., Papadimitriou, E., Makropoulos, K., Voulgaris, N., Papaioannou, C., 2000. Microseismicity and faulting geometry in the Gulf of Corinth (Greece). Geophysical Journal International 141 (2), 438–456. doi:10.1046/j.1365-246x.2000.00092.x.

Kaverina, A., Dreger, D., Price, E., 2002. The combined inversion of seismic and geodetic data for the source process of the 16 October 1999 Mw 7.1 Hector Mine, California, Earthquake. Bulletin of the Seismological Society of America 92 (4), 1266–1280. doi:10.1785/0120000907.

Kiratzi, A., 2011. The 6 September 2009 Mw5.4 earthquake in Eastern Albania – FYROM Border: focal mechanisms, slip model, ShakeMap. Turkish Journal of Earth Sciences 20 (4), 475–488.

Kiratzi, A., Louvari, E., 2003. Focal mechanisms of shallow earthquakes in the Aegean Sea and the surrounding lands determined by waveform modelling: a new database. Journal of Geodynamics 36 (1–2), 251–274. doi:10.1016/s0264-3707(03)00050-4.

Kiratzi, A., Sokos, E., Ganas, A., Tselentis, A., Benetatos, C., Roumelioti, Z., Serpetsidaki, A., Andriopoulos, G., Galanis, O., Petrou, P., 2008. The April 2007 earthquake swarm near Lake Trichonis and implications for active tectonics in western Greece. Tectonophysics 452 (1–4), 51–65. doi:10.1016/j.tecto.2008.02.009.

Klein, F.W., 2002. User's guide to HYPOINVERSE-2000, a Fortran Program to solve for earthquake locations and magnitudes. U.S.G.S. Open File Report 02–171 Version 1.0 (2002)http://geopubs.wr.usgs.gov/open-file/of02-171/. 123 pp.

Latorre, D., Virieux, J., Monfret, T., Monteiller, V., Vanorio, T., Got, J.L., Lyon-Caen, H., 2004. A new seismic tomography of Aigion area (Gulf of Corinth, Greece) from the 1991 data set. Geophysical Journal International 159 (3), 1013–1031. doi:10.1111/j.1365-246X.2004.02412.x.

Lyon-Caen, H., Bernard, P., Deschamps, A., Lambotte, S., Briole, P., 2010. The January-February 2010 Pyrgos seismic swarm: a possible activation of the deep Psathopyrgos normal fault (western Corinth rift) ? European Seismological Commision 32nd General Assembly, Montpellier, France.

Mai, P.M., Spudich, P. and Boatwright, J., 2005. Hypocenter Locations in Finite-Source Rupture Models. Bull. Seismol. Soc.Am., 95(3): 965–980. doi:10.1785/0120040111.

McKenzie, D., 1972. Active tectonics of the Mediterranean region. Geophysical Journal of the Royal Astronomical Society 30 (2), 109–185. doi:10.1111/j.1365-246X.1972.tb02351.x.

Melis, N.S., Brooks, M., Pearce, R.G., 1989. A microearthquake study in the Gulf of Patras region, western Greece, and its seismotectonic interpretation. Geophysical Journal International 98 (3), 515–524. doi:10.1111/j.1365-246X.1989.tb02286.x.

Pacchiani, F., Lyon-Caen, H., 2010. Geometry and spatio-temporal evolution of the 2001 Agios Ioanis earthquake swarm (Corinth Rift, Greece). Geophysical Journal International 180 (1), 59–72. doi:10.1111/j.1365-246X.2009.04409.x.

Papanikolaou, D., Chronis, G., Lykousis, V., Sakellariou, D., Papoulia, I., 1997. Submarine neotectonic structure of W. Korinthiakos Gulf and geodynamic phenomena of the Egion earthquake. Proceedings of 5th Hellenic Congress of Oceanography & Fisheries, Volume I. Kavala, Greece, pp. 415–418.

Papazachos, B.C., Karakostas, B.G., Kiratzi, A.A., Papadimitriou, E.E., Papazachos, C.B., 1998. A model for the 1995 Kozani-Grevena seismic sequence. Journal of Geodynamics 26 (2–4), 217–231. doi:10.1016/s0264-3707(97)00050-1.

Rigo, A., Lyon-Caen, H., Armijo, R., Deschamps, A., Hatzfeld, D., Makropoulos, K., Papadimitriou, P., Kassaras, I., 1996. A microseismic study in the western part of the Gulf of Corinth (Greece): implications for large-scale normal faulting mechanisms. Geophysical Journal International 126 (3), 663–688.

Roberts, G.P., Koukouvelas, I., 1996. Structural and seismological segmentation of the Gulf of Corinth fault system: implications for models of fault growth. Annals of Geophysics 39 (3).

Sokos, E.N., Zahradnik, J., 2008. ISOLA a Fortran code and a Matlab GUI to perform multiple-point source inversion of seismic data. Computers and Geosciences 34 (8), 967–977. doi:10.1016/j.cageo.2007.07.005.

Somerville, P., Irikura, K., Graves, R., Sawada, S., Wald, D., Abrahamson, N., Iwasaki, Y., Kagawa, T., Smith, N., Kowada, A., 1999. Characterizing crustal earthquake slip models for the prediction of strong ground motion. Seismological Research Letters 70 (1), 59–80. doi:10.1785/gssrl.70.1.59.

Sorel, D., 2000. A Pleistocene and still-active detachment fault and the origin of the Corinth-Patras rift, Greece. Geology 28 (1), 83–86. doi:10.1130/0091-7613(2000)28<83:apasdf>2.0.co;2.

Stefatos, A., Papatheodorou, G., Ferentinos, G., Leeder, M., Collier, R., 2002. Seismic reflection imaging of active offshore faults in the Gulf of Corinth: their seismotectonic significance. Basin Research 14 (4), 487–502. doi:10.1046/j.1365-2117.2002.00176.x.

Toda, S., Stein, R.S., Richards-Dinger, K., Bozkurt, S.B., 2005. Forecasting the evolution of seismicity in southern California: animations built on earthquake stress transfer. Journal of Geophysical Research 110 (B5), B05S16. doi:10.1029/2004jb003415.

Valkaniotis, S., 2009. Correlation between Neotectonic structures and Seismicity in the broader area of Gulf of Corinth (Central Greece). PhD Thesis, Aristotle University of Thessaloniki, Thessaloniki.

Vaníček, P., 1971. Further development and properties of the spectral analysis by least-squares. Astrophysics and Space Science 12 (1), 10–33. doi:10.1007/bf00656134.

Vassilakis, E., Royden, L., Papanikolaou, D., 2011. Kinematic links between subduction along the Hellenic trench and extension in the Gulf of Corinth, Greece: a multidisciplinary analysis. Earth and Planetary Science Letters 303 (1–2), 108–120. doi:10.1016/j.epsl.2010.12.054.

Waldhauser, F., 2001. hypoDD: a computer program to compute double-difference earthquake locations. USGS Open File Rep, pp. 01–113http://geopubs.wr.usgs.gov/open-file/of01-113/.

Zahradnik, J., Gallovic, F., 2010. Toward understanding slip inversion uncertainty and artifacts. Journal of Geophysical Research 115 (B9), B09310. doi:10.1029/2010jb007414.

Zahradnik, J., Jansky, J., Sokos, E., Serpetsidaki, A., Lyon-Caen, H., Papadimitriou, P., 2004. Modeling the ML4.7 mainshock of the February–July 2001 earthquake sequence in Aegion, Greece. Journal of Seismology 8 (2), 247–257. doi:10.1023/B:JOSE.0000021376.21087.2d.

Zahradnik, J., Gallovic, F., Sokos, E., Serpetsidaki, A., Tselentis, A., 2008a. Quick fault–plane identification by a geometrical method: application to the MW 6.2 Leonidio earthquake, 6 January 2008, Greece. Seismological Research Letters 79 (5), 653–662. doi:10.1785/gssrl.79.5.653.

Zahradnik, J., Jansky, J., Plicka, V., 2008b. Detailed waveform inversion for moment tensors of M~4 events: examples from the Corinth Gulf, Greece. Bulletin of the Seismological Society of America 98 (6), 2756–2771. doi:10.1785/0120080124.

Zahradnik, J., Sokos, E., Tselentis, G.A., Martakis, N., 2008c. Non-double-couple mechanism of moderate earthquakes near Zakynthos, Greece, April 2006; explanation in terms of complexity. Geophysical Prospecting 56 (3), 341–356. doi:10.1111/j.1365-2478.2007.00671.x.